




## Open Archive Toulouse Archive Ouverte (OATAO)

OATAO is an open access repository that collects the work of Toulouse researchers and makes it freely available over the web where possible

This is an author's version published in: <http://oatao.univ-toulouse.fr/23053>

**Official URL:** <https://doi.org/10.1021/nn404954s>

### **To cite this version:**

Sanchez, Claire and El Hajj Diab, Darine and Connord, Vincent and Clerc, Pascal and Meunier, Etienne and Pipy, Bernard and Payre, Bruno and Tan, Reasmey P. and Gougeon, Michel  and Carrey, Julian and Gigoux, Véronique and Fourmy, Daniel *Targeting a G-Protein-Coupled Receptor Overexpressed in Endocrine Tumors by Magnetic Nanoparticles To Induce Cell Death.* (2014) ACS Nano, 8 (2). 1350-1363. ISSN 1936-0851

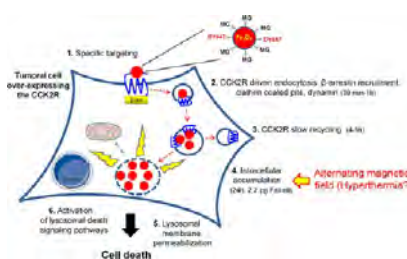
Any correspondence concerning this service should be sent to the repository administrator: [tech-oatao@listes-diff.inp-toulouse.fr](mailto:tech-oatao@listes-diff.inp-toulouse.fr)

# Targeting a G-Protein-Coupled Receptor Overexpressed in Endocrine Tumors by Magnetic Nanoparticles To Induce Cell Death

Claire Sanchez,<sup>†</sup> Darine El Hajj Diab,<sup>†,#</sup> Vincent Connord,<sup>\*,#</sup> Pascal Clerc,<sup>†</sup> Etienne Meunier,<sup>§</sup> Bernard Pipy,<sup>§</sup> Bruno Payré,<sup>‡</sup> Reasmeay P. Tan,<sup>‡</sup> Michel Gougeon,<sup>||</sup> Julian Carrey,<sup>‡</sup> Véronique Gigoux,<sup>†</sup> and Daniel Fourmy<sup>†,\*</sup>

<sup>†</sup>EA 4552, Université de Toulouse 3, Toulouse, France, <sup>‡</sup>Laboratoire de Physique et Chimie des Nano-Objets, INSA/CNRS, Toulouse, France, <sup>§</sup>EA2405, Université de Toulouse 3, Toulouse, France, <sup>‡</sup>CMEAB, Faculté de Médecine, Université de Toulouse 3, Toulouse, France, and <sup>||</sup>CIRIMAT, Université de Toulouse 3/CNRS, Toulouse, France. <sup>#</sup>D. El Hajj Diab and V. Connord equally contributed to this work.

**ABSTRACT** Nanotherapy using targeted magnetic nanoparticles grafted with peptidic ligands of receptors overexpressed in cancers is a promising therapeutic strategy. However, nanoconjugation of peptides can dramatically affect their properties with respect to receptor recognition, mechanism of internalization, intracellular trafficking, and fate. Furthermore, investigations are needed to better understand the mechanism whereby application of an alternating magnetic field to cells containing targeted nanoparticles induces cell death. Here, we designed a nanoplatform (termed MG-IONP-DY647) composed of an iron oxide nanocrystal decorated with a ligand of a G-protein coupled receptor, the cholecystokinin-2 receptor (CCK2R) that is overexpressed in several malignant cancers. MG-IONP-DY647 did not stimulate inflammasome of Raw 264.7 macrophages. They recognized cells expressing CCK2R with a high specificity, subsequently internalized *via* a mechanism involving recruitment of  $\beta$ -arrestins, clathrin-coated pits, and dynamin and were directed to lysosomes. Binding and internalization of MG-IONP-DY647 were dependent on the density of the ligand at the nanoparticle surface and were slowed down relative to free ligand. Trafficking of CCK2R internalized with the nanoparticles was slightly modified relative to CCK2R internalized in response to free ligand. Application of an alternating magnetic field to cells containing MG-IONP-DY647 induced apoptosis and cell death through a lysosomal death pathway, demonstrating that cell death is triggered even though nanoparticles of low thermal power are internalized in minute amounts by the cells. Together with pioneer findings using iron oxide nanoparticles targeting tumoral cells expressing epidermal growth factor receptor, these data represent a solid basis for future studies aiming at establishing the proof-of-concept of nanotherapy of cancers using ligand-grafted magnetic nanoparticles specifically internalized *via* cell surface receptors.



**KEYWORDS:** iron oxide nanoparticles · cholecystokinin-2 receptor · endocrine tumors · internalization · intracellular trafficking · alternating magnetic field · lysosomal cell death pathways

Cancer is a leading cause of death, with millions of new people diagnosed with cancer every year, making the development of new methods for efficient and specific delivery of diagnostic and therapeutic agents to tumors a permanent challenge. Over the past two decades, the introduction of targeted cancer therapeutics in the clinic has been a major breakthrough in cancer therapy. Currently, targeted delivery of diagnosis and/or therapeutic agents to tumoral cells uses biological markers selectively expressed or at least overexpressed in tumors relative to healthy surrounding and distant tissues.<sup>1,2</sup>

In this context, much attention is focused toward the development of strategies combining molecular targeting and nanoparticle delivery.<sup>1,3</sup> Among the wide range of available nanoparticles, magnetic nanoparticles have emerged as potential biocompatible systems for cancer detection by magnetic resonance imaging (MRI) and for targeted cancer therapy.<sup>3–7</sup> Indeed, magnetic nanoparticles offer the theoretical potential to be driven to the tumors by grafting the nanoparticles with ligands or antibodies recognizing receptors or antigens overexpressed in tumors.<sup>1</sup> *In vivo*, targeted magnetic nanoparticles injected intravenously

\* Address correspondence to Daniel.Fourmy@inserm.fr.

10.1021/nn404954s

---

accumulate within the tumor, where they can act as a thermoablative agent upon application of an alternating magnetic field. In addition, targeted magnetic nanoparticles can serve as nanocarriers of cytotoxic agents through the body, enabling their preferred delivery to primary and metastatic tumors.<sup>1</sup> Interestingly, targeted magnetic nanoparticles offer the opportunity of combining targeted hyperthermia therapy and chemotherapy. Using such therapeutic strategies, exposure of tumoral tissues to therapeutic agents should be optimized, whereas that of healthy tissues should be minimized.

Iron oxide nanoparticles (IONPs), which display low toxicity in humans, are the subject of renewed interest in the perspective of nanotherapy of cancers.<sup>8</sup> A first field of investigation aims at increasing our knowledge about engineering targeted iron oxide nanoparticles to enhance their ability to efficiently reach solid tumors after systemic administration. Escape of the nanoparticles from the reticuloendothelial system, their extravascular transport to the tumor, and subsequent tumor penetration and accumulation still represent important challenges, although key breakthroughs were recently made.<sup>9,10</sup> Another important point concerns the specificity of targeted nanoparticles, which is often far from expected, including in cultured cells *in vitro*. In fact, targeting is usually obtained through the chemical grafting of ligands (in the case of receptor targeting) to the surface of the nanoparticles. Yet, this nanoconjugation can dramatically modify properties of the ligands with respect to recognition parameters (kinetics, specificity, affinity), mechanism of internalization, intracellular trafficking, and fate.<sup>11–13</sup> A second field of active research is related to magnetic hyperthermia and mechanisms at the origin of cancer cell death.<sup>13–15</sup> *In vivo* studies with transplanted tumors in animals and even clinical trials with prostate cancer or brain tumor patients have provided the proof-of-concept of hyperthermia therapy of cancers with IONPs.<sup>16,17</sup> However, in most of the *in vivo* investigations so far reported, high amounts of IONPs were injected intravenously or even directly injected into the tumors. Therefore, results obtained in these studies cannot be generalized to targeted IONPs which are actively and specifically internalized in lower amounts by tumoral cells through their cell-surface target.

Interestingly, magnetic iron oxide nanoparticles targeting epidermal growth factor (EGF) receptor were recently shown to be internalized by tumoral cells and to kill the cells upon application of an alternating magnetic field.<sup>13,14,18</sup> Cell death was achieved without a perceptible temperature rise and occurred through a mechanism involving lysosomal death pathways.<sup>13,14,18</sup> Such data stimulate research aimed at developing strategies of targeted nanotherapy of cancers overexpressing other cell surface receptors.

The aim of our study was to design and evaluate a hybrid system (termed MG-IONP-DY647) composed of an iron oxide nanocrystal decorated with a peptidic ligand of the cholecystokinin-2 receptor (CCK2R). The CCK2R was chosen as an example of targeted receptor because this seven-transmembrane domain peptide receptor is expressed at high incidence and density in cancers such as medullary thyroid carcinomas, small cell lung cancers (SCLC), gastrointestinal stromal tumors (GIST), and insulinomas.<sup>19–21</sup> Moreover, CCK2R undergoes rapid internalization and subsequent trafficking to lysosomes following stimulation by its equally potent natural ligands, gastrin and cholecystokinin (CCK).<sup>22,23</sup> Recently, a number of radiolabeled replicates of CCK or gastrin have been developed, with the indication of receptor-targeted tumor imaging and therapy, on the example of imaging probes that are currently used in the clinic to detect neuroendocrine tumors overexpressing somatostatin receptors.<sup>19,20</sup> However, so far, none of these CCK or gastrin radiolabels have been approved for clinical use, as their renal retention and expected radiotoxicity remain a major drawback.

We demonstrated the ability of MG-IONP-DY647 to specifically target cells expressing CCK2R, characterized internalization and intracellular trafficking of the nanoparticles, and finally used them as a targeted therapeutic agent to induce tumoral cell death through a cell death lysosomal pathway. Thus, we here confirm that a small amount of nanoparticles displaying a small heating power is sufficient to induce cell death upon an alternating magnetic field. These data are very promising in light of the recent concept that lysosomal membrane permeabilization could be an effective way to kill apoptosis-resistant cancer cells.<sup>24</sup>

## RESULTS

**Preparation of Gastrin-Decorated Iron Oxide Magnetic Nanoparticles (MG-IONP-DY647).** In order to selectively target CCK2R with minor cross-recognition of CCK1R, which is also frequently expressed in tumors,<sup>19</sup> gastrin, a selective CCK2R ligand, was chosen as a cross-linked peptide to IONPs. Previous data showing that radiolabeled gastrin injected into animals is abundantly retained by the kidney due to the presence of five glutamic acids in the middle of the peptidic sequence were taken into account for the design of the gastrin replicate (Figure 1a).<sup>25,26</sup> Thus, a synthetic replicate of gastrin, termed MG, which contains the pharmacophore of natural gastrin but has its Glu-Glu-Glu-Glu-Glu sequence replaced by Cys-Lys-Ser-Ser-Glu was synthesized. Importantly, this peptide shares its C-terminal bioactive sequence with the natural agonist CCK, which is used as reference peptide for CCK2R internalization studies (Figure 1a). Control experiments established that MG bound to CCK2R with only 7.3-fold lower affinity than CCK and stimulated production of



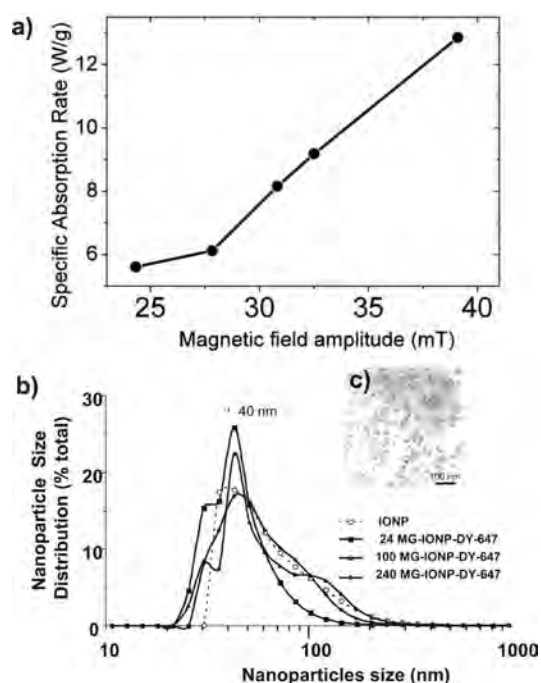


**Figure 2.** Physicochemical properties of MG-IONP-DY647. (a) Specific absorption rate of a mother solution of magnetic nanoparticles measured at a frequency of 275 kHz as a function of the magnetic field amplitude. Solution concentration was 5.9 mg Fe/mL. (b) Dynamic light scattering analysis of MG-IONP-DY647 in solution (0.1 mg Fe/mL) in RPMI 1640 medium containing 0.5% FBS. The iron nanoparticle suspension was sonicated for 10 min on ice before analysis. (c) Transmission electron microscopy analysis of MG-IONP-DY647 showing size homogeneity of IONP nanoparticles. An average size of  $8.7 \pm 1.6$  nm was calculated.

processes.<sup>4,27,28</sup> Incubation of MG-IONP-DY647 *in vitro* with Raw 264.7 mouse leukemic monocyte macrophages or with mouse peritoneal macrophages resulted in rapid and abundant uptake of nanoparticles (Figure 3a,b). Then, activation of macrophages was tested on both untreated and LPS-stimulated Raw 264.7 cells by measuring the secretion of the cytokine IL-1 $\beta$  (Figure 3c). We found that in contrast to silica nanoparticles recognized as potent inducers of inflammasome and which elicit release of the cytokine IL-1 $\beta$ ,<sup>29</sup> MG-IONP-DY647 at concentrations up to 2 mg/mL did not trigger significant release of IL-1 $\beta$  from both untreated and LPS-primed Raw 264.7 cells (Figure 3c). These first results are in favor of biocompatibility of MG-IONP-DY647.

**Specific Targeting of HEK293 Cells Expressing CCK2R by MG-IONP-DY647 and Intracellular Trafficking of the Nanoparticles.** Our targeting strategy using MG-IONP-DY647 requires specific recognition of nanoconjugated MG molecules by the CCK2R expressed at the cell surface and internalization of the nanoparticles through the endocytotic machinery usually involved in CCK2R endocytosis. Yet, nanoconjugated MG molecules might modify its pharmacological properties. We therefore characterized binding and internalization of MG-IONP-DY647 in HEK293 cells expressing CCK2R, namely, Flp-In

CCK2R-293, previously used to precisely delineate agonist-induced CCK2R internalization.<sup>22</sup>

Confocal microscopy images show slow binding of MG-IONP-DY647 to the membrane of Flp-In CCK2R-293 cells, which were progressively illuminated at their surface upon contact with MG-IONP-DY647 (Figure 4a). This binding of MG-IONP-DY647 to the cell surface was slower than previously appreciated with unconjugated ligands.<sup>22</sup> Following binding, MG-IONP-DY647 abundantly internalized over the time (Figure 4a). Only minor nonspecific binding/uptake of red fluorescence was seen on HEK293 cells lacking CCK2R (Figure 4c) or on Flp-In CCK2R-293 cells incubated in the presence of a saturating concentration (1  $\mu$ M) of CCK (Figure 4b).

Subcellular localization of MG-IONP-DY647 was assessed by transmission electron microscopy. As illustrated in Figure 4d, MG-IONP-DY647 were located in endocytotic vesicles. The number of nanoparticles in small vesicles, as well as the number of vesicles containing nanoparticles, increased within the first 2–3 h of incubation. Then, the size of vesicles containing MG-IONP-DY647 clearly increased, showing intracellular accumulation and storage of highly concentrated nanoparticles (Figure 4d).

Given that nanoparticles can enter cells through several ways, the initial mechanism of MG-IONP-DY647 internalization was investigated. We previously showed that the molecular mechanism of agonist-induced internalization of CCK2R involves recruitment of nonvisual arrestins, clathrin-coated pits, and dynamin.<sup>22</sup> In Figure 5a, confocal microscopy imaging of cells transiently expressing GFP-tagged  $\beta$ -arrestin2 incubated with MG-IONP-DY647 shows fluorescent nanoparticles in intracellular vesicles containing  $\beta$ -arrestin2. Furthermore, internalization of MG-IONP-DY647 was blocked in the presence of chlorpromazine, a clathrin inhibitor, at 75  $\mu$ M (Figure 5c; dose–response effect shown in the Supporting Information, Figure 2). In line with this result, incubation of MG-IONP-DY647 with cells transiently expressing eYFP-tagged clathrin polypeptide showed abundant intracellular co-localization (Figure 5d). Furthermore, MG-IONP-DY647 internalization was inhibited in the presence of the dynamin inhibitor dynasore (Figure 5e). The possibility of uptake through caveoles was also examined by testing the effect of filipin, an inhibitor of caveoles. However, abundant internalization of MG-IONP-DY647 in the presence of filipin was still observed, supporting that MG-IONP-DY647 endocytosis did not significantly occur through caveoles in Flp-In CCK2R-293 cells (Figure 5f).

Intracellular trafficking of internalized MG-IONP-DY647 was then investigated. First, co-localization of MG-IONP-DY647 with CCK2R during intracellular trafficking was studied and quantified in cells expressing GFP-tagged CCK2R. As shown in Figure 6a and b, internalized MG-IONP-DY647, as well as CCK-DY647, co-localized with CCK2R in endocytotic vesicles. However,



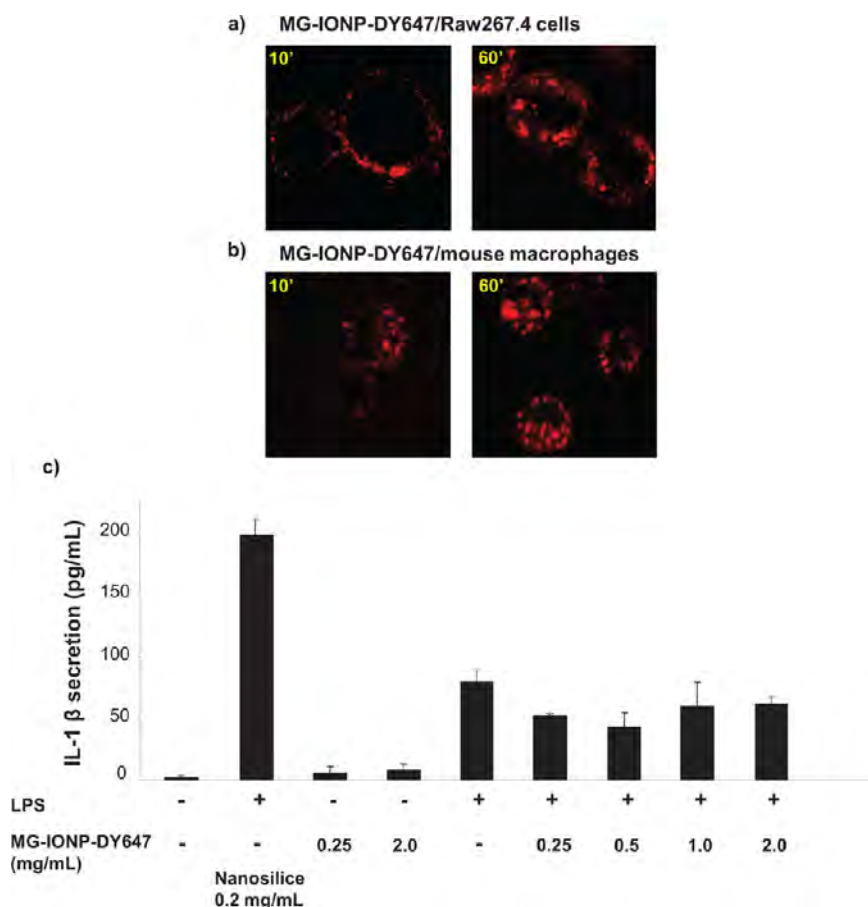


**Figure 3. Absence of inflammasome activation of macrophages by MG-IONP-DY647.** (a) Uptake of nanoparticles by Raw 264.7 mouse leukemic monocyte macrophages. Confocal microscopy images illustrating Raw 264.7 cells incubated with MG-IONP-DY647 (8  $\mu\text{g Fe/mL}$ ) for indicated times at 37  $^{\circ}\text{C}$ . (b) Uptake of nanoparticles by mouse peritoneal macrophages. Resident peritoneal cells were harvested by washing the peritoneal cavity of female Swiss mice with sterile NaCl 0.9%. Two hours after seeding, macrophages were incubated with MG-IONP-DY647 (8  $\mu\text{g Fe/mL}$ ) for indicated times at 37  $^{\circ}\text{C}$ . (c) Assay of IL-1 $\beta$  secretion. Untreated or LPS-primed Raw 264.7 cells were stimulated with increasing concentrations of MG-IONP-DY647 or with nanosilica (0.2 mg/mL) for 6 h at 37  $^{\circ}\text{C}$ . IL-1 $\beta$  release in culture supernatant was assayed with an ELISA kit. Results are mean  $\pm$  SEM of three separate experiments.

the time-courses of co-localization differed. Indeed, comparing Figure 6a and b shows that co-localization between CCK-DY647 and CCK2R was persistent, whereas progressive and partial dissociation between MG-IONP-DY647 and GFP-tagged CCK2R was noted at earlier times. These results suggest that nanoconjugation of MG to magnetic nanoparticles affects the trafficking properties of internalized CCK2R and perhaps enables the CCK2R to recycle faster than when stimulated with unconjugated ligand. To examine this possibility, we evaluated co-localization of CCK2R stimulated with MG-IONP-DY647 *versus* CCK-DY647 in vesicles expressing Rab11, a small GTPase of recycling vesicles.<sup>30</sup> As represented in Figure 7a, localization of CCK2R-GFP in Rab11-DsRed containing vesicles was maximal after 4 h of incubation with MG-IONP-DY647 and then slightly decreased. When stimulated with CCK-DY647 (or with MG-DY647, not shown), the localization profile of CCK2R in DsRed-tagged Rab-11 positive vesicles was significantly different, with a slower increase to a maximum after 5 h of incubation.

Thus, CCK2R stimulated with MG-IONP-DY647 seems to recycle faster than when stimulated with the non-conjugated ligands; however, the recycling takes several hours, as previously demonstrated.<sup>22</sup>

Last, the intracellular fate of MG-IONP-DY647 was analyzed using the lysosome staining reagent LysoTracker and by incubating MG-IONP-DY647 with cells transiently expressing DsRed-tagged Rab7, a small GTPase of late endosomes and lysosomes. As illustrated in Figure 7b, a high proportion of LysoTracker-stained lysosomes contained MG-IONP-DY647 after times longer than 1 h of incubation, and co-localization images between MG-IONP-DY647 and Rab7-Ds-Red were observed in most cells (Figure 7c).

Together, this set of results demonstrates that nanoconjugation of MG to IONPs enables active endocytosis of the nanoparticles, and, by facilitating separation of the receptor from endocytotic vesicles, nanoconjugation slightly accelerates the presence of the targeted receptor in slowly recycling vesicles. Importantly, MG-IONP-DY647 uptake by cells remains fully dependent on CCK2R

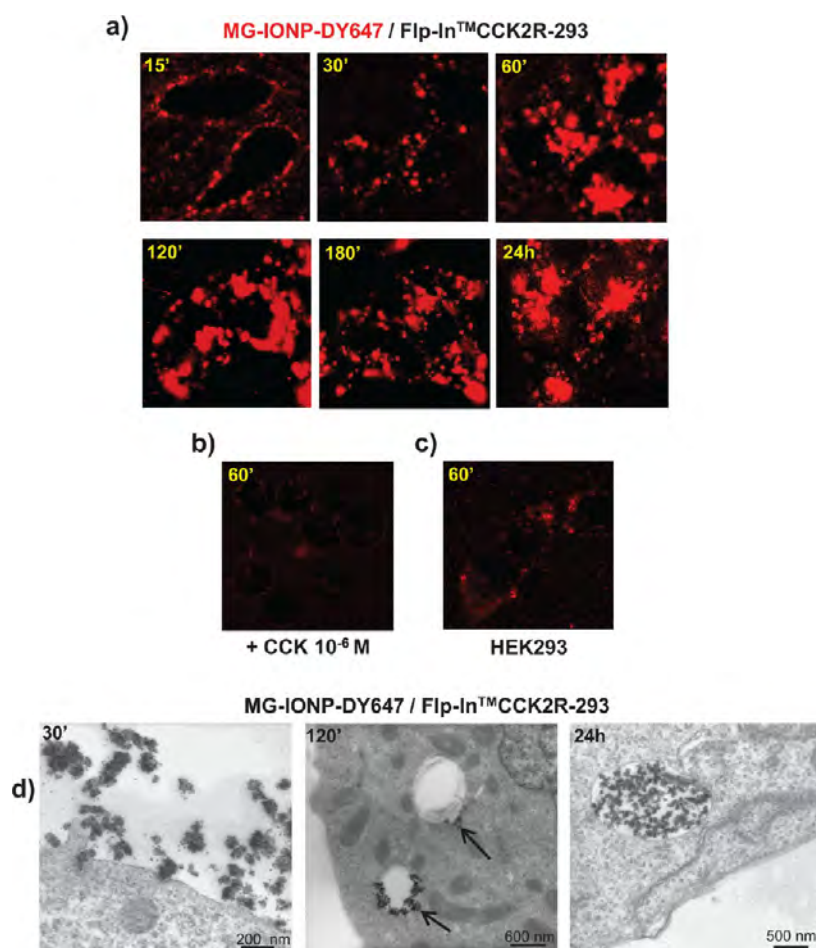


**Figure 4.** MG-IONP-DY647 specifically bind to Flp-In CCK2R-293 cells and are subsequently internalized and trapped within the cells. (a, b, c) Confocal microscopy images illustrating specificity of uptake of MG-IONP-DY647. (a) HEK293 cells expressing CCK2R (Flp-In CCK2R-293) were incubated at 37 °C with MG-IONP-DY647 alone (8  $\mu$ g Fe/ml) or (b) in the presence of 1  $\mu$ M CCK. (c) HEK293 lacking CCK2R were incubated with MG-IONP-DY647. (d) Electron microscopy analysis of MG-IONP-DY647 internalization in Flp-In CCK2R-293 cells. Cells were incubated with nanoparticles (8  $\mu$ g Fe/mL) for indicated times at 37 °C. Arrows depict the presence of nanoparticles in endocytotic vesicles.

internalization and involves recruitment of  $\beta$ -arrestin2, clathrin-coated pits, and dynamin. Furthermore, internalized MG-IONP-DY647 are directed to lysosomes, where they are trapped for times up to 24 h.

**Targeting of InR1G9-CCK2R Tumoral Endocrine Cells by MG-IONP-DY647 Nanoparticles.** Tumoral cells display profound modifications relative to “normal” cells, which affect the plasma membrane, intracellular trafficking as well as lysosomal volume, composition, and cellular distribution.<sup>31</sup> Therefore, we next characterized the behavior of MG-IONP-DY647 toward tumoral cells expressing or not CCK2R. Specificity and kinetics of MG-IONP-DY647 binding, accumulation in lysosomes, and dependency on the density of MG at the nanoparticle surface were precisely investigated on the tumoral endocrine cell line expressing CCK2R, namely, InR1G9-CCK2R.<sup>32</sup>

Confocal microscopy observations confirmed specific binding of MG-IONP-DY647 to the tumoral cells and subsequent internalization, as no significant uptake was detected in InR1G9 lacking CCK2R or InR1G9-CCK2R incubated in the presence of 1  $\mu$ M

CCK (Supporting Information, Figure 3a,b,c). MG-IONP-DY647 binding and internalization determined by FACS indicates that the amount of MG-IONP-DY647 taken up by the cells increased with the time of incubation but much slower than that of CCK-DY647, which was maximum between 1 and 3 h of incubation and then decreased (Figure 8). Furthermore, the amount of bound and internalized MG-IONP-DY647 by the cells increased proportionally to MG density at the surface of the nanoparticles. After 24 h of incubation, magnetic measurements showed an amount of  $2.2 \pm 0.2$  pg of iron per cell incubated with nanoparticles grafted with 100 molecules of MG (termed 100MG-IONP-DY647 in Figures 8 and 9). FACS quantifications also confirmed high specificity of targeting since nanoparticles without grafted MG (termed IONP-DY647 in Figure 8) were taken up in very low amounts by InR1G9-CCK2R tumoral cells and MG-IONP-DY647 were poorly taken up by InR1G9 tumoral cells lacking CCK2R at their surface ( $9.1 \pm 2.1\%$  of nonspecific binding after 24 h of incubation, not shown). Finally,

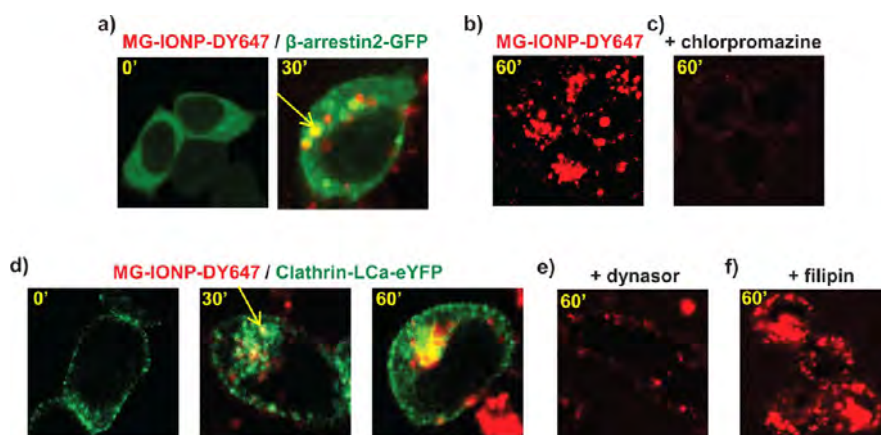


**Figure 5.** Internalization of MG-IONP-DY647 in Flp-In CCK2R-293 cells occurs through CCK2R endocytotic machinery. (a) MG-IONP-DY647 internalize through recruitment of  $\beta$ -arrestin2. Flp-In CCK2R-293 cells transiently expressing  $\beta$ -arrestin-2-GFP were incubated with MG-IONP-DY647. At initial time,  $\beta$ -arrestin-2 (in green) was uniformly scattered in the cytoplasm, whereas after 30 min of stimulation with nanoparticles, it was also seen in endocytotic vesicles together with MG-IONP-DY647 (in yellow). (b, c, d) MG-IONP-DY647 internalize via clathrin-coated pits. Flp-In CCK2R-293 cells were incubated at 37 °C for 60 min (b) with MG-IONP-DY647 alone or (c) in the presence of the clathrin-coated-pits inhibitor chlorpromazine (75  $\mu$ M). Dose-response effect of chlorpromazine is shown in Supporting Information Figure 2. (d) Flp-In CCK2R-293 cells transiently expressing clathrin-LCa-eYFP were incubated with MG-IONP-DY647 at 37 °C. Co-localization between MG-IONP-DY647 and clathrin-LCa-eYFP is seen in yellow. (e) MG-IONP-DY647 internalization requires dynamin. Flp-InCCK2R-293 cells were incubated with MG-IONP-DY647 in the presence of dynasor (160  $\mu$ M). Dynasor efficiently inhibited internalization. (f) MG-IONP-DY647 internalization is not sensitive to filipin, an inhibitor of caveoles. Flp-In CCK2R-293 cells were incubated with MG-IONP-DY647 in the presence of filipin (10  $\mu$ M). No significant inhibition of internalization could be observed.

lysosome occupancy by MG-IONP-DY647 (illustrated in the Supporting Information, Figure 3d) was quantified by confocal microscopy. Kinetics of accumulation of MG-IONP-DY647 in lysosomes were in agreement with that of binding/internalization (Figure 9). After 24 h of incubation, lysosome occupancy by nanoparticles grafted with 24, 100, or 240 MG molecules reached  $31.6 \pm 1.9\%$ ,  $46.8 \pm 0.7\%$ , or  $49.8 \pm 1.8\%$ , respectively. No significant presence of nanoparticles without MG (termed IONP-DY647) could be noticed in lysosomes after 24 h of incubation (Figure 9). On the other hand, lysosome occupancy by unconjugated CCK-DY647 was maximal at 1 and 3 h of incubation and then dramatically decreased to almost disappear at 24 h, suggesting ligand degradation in lysosomes.

**Internalized MG-IONP-DY647 by Tumoral Cells Induce Apoptosis and Cause Cell Death upon an Alternating Magnetic Field.** Having assessed the ability of MG-IONP-DY647 to specifically target endocrine tumoral cells expressing CCK2R and to abundantly accumulate in lysosomes of these cells, the next step was to test the ability of the nanoparticles to induce cell death upon exposure to an alternating magnetic field. For this purpose, InR1G9-CCK2R tumoral cells incubated with MG-IONP-DY647 for 24 h were maintained at 37 °C and exposed to an alternating magnetic field (275 kHz, 40 or 52 mT for 2 h). Controls were composed of cells having internalized ligand without nanoparticles (CCK-DY647) and cells having internalized MG-IONP-DY647 but that were not exposed to the alternating magnetic field. In preliminary experiments, we also checked that cells incubated with nanoparticles without grafted gastrin and that did not internalize these nanoparticles (Figure 9)

behaved similarly to cells having internalized CCK-DY647 (not illustrated).

The impact of magnetic field treatment was determined by counting cells labeled by FITC-tagged annexin V and/or propidium iodure, which identified early apoptotic, late apoptotic, and necrotic cells, respectively. As shown in Figure 10, application of the alternating magnetic field during 2 h caused the cells to enter into apoptosis. The total number of apoptotic cells reached  $17.1 \pm 1.6\%$  at 40 mT amplitude and  $36.4 \pm 5.5\%$  at 52 mT amplitude. In control cells having internalized unconjugated CCK-DY647 and exposed to the same magnetic field amplitudes, apoptotic cells represented  $3.0 \pm 0.7\%$  and  $11.2 \pm 0.4\%$  of the total cell population. The number of necrotic cells, namely, cells that became positive for propidium iodure labeling only, was not significant with a magnetic field of 40 mT, whereas it increased up to 5.9% at 52 mT. Determination of cell survival 24 h after magnetic field exposure using the MTT assay indicated that a magnetic field of 40 or 52 mT killed  $26.9 \pm 7.6\%$  and  $67.1 \pm 9.9\%$  of tumoral cells, respectively. It is worthy to note that a magnetic field of 52 mT affected the viability of cells that had not accumulated nanoparticles, whereas an amplitude of 40 mT had a minor effect (Figure 10a,b).

Since a recent study with EGF-grafted nanoparticles documented that an alternating magnetic field caused lysosome membrane permeabilization, we determined whether it was also the case with MG-IONP-DY647 nanoparticles. First, the effect of a magnetic field was evaluated on lysosome staining with LysoTracker Red. As evidenced in Figure 10c, exposure of cells containing MG-IONP-DY647 to a magnetic field of 40 or 52 mT



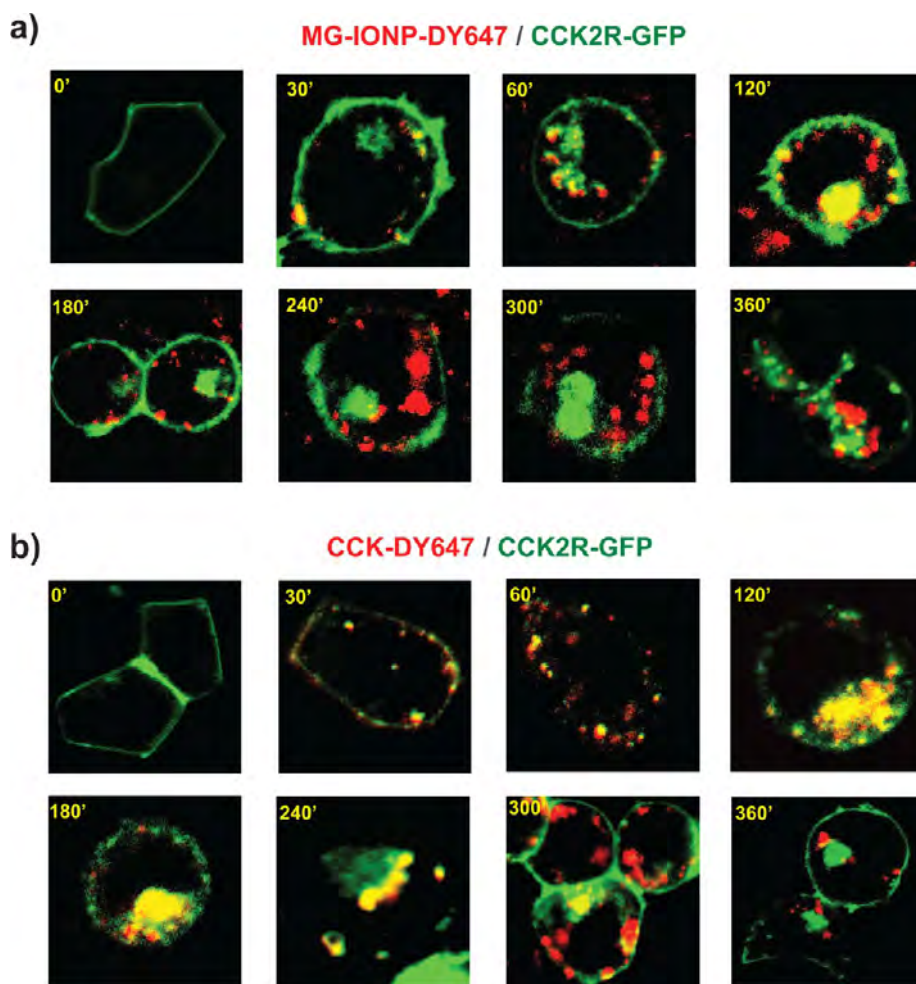


Figure 6. MG-IONP-DY647 dissociate faster from internalized CCK2R than unconjugated fluorescent ligand. Confocal microscopy images illustrating changes in co-localization between MG-IONP-DY647 and CCK2R-GFP over time. HEK293 cells transiently expressing CCK2R-GFP were incubated with (a) MG-IONP-DY647 (8  $\mu$ g Fe/ml) or (b) CCK-DY647 (50 nM). Merged images show that CCK2R-GFP does not co-localize with MG-IONP-DY647 as long as CCK-DY647 does.

induced drops of lysosome stain, suggesting leaking of lysosome content (see Supporting Information, Figure 4 for an illustration). Furthermore, the effect of the magnetic field on apoptosis was almost totally reversed by E64d, an inhibitor of cysteine proteases such as lysosomal cathepsins B, L, C, H, and P (Figure 10a). Pepstatin A, an inhibitor of aspartyl peptidases such as lysosomal cathepsin D, did not reverse cell death (not shown). The effect of the magnetic field on apoptosis was also significantly diminished by chloroquine, a weak base affecting activity of lysosomes and autophagy (at 40 mT, amount of apoptotic cells:  $6.8 \pm 0.5\%$  in the presence of chloroquine *versus*  $17.1 \pm 1.6\%$  in the absence of chloroquine, not illustrated).

This set of results shows that application of an alternating magnetic field to InR1G9 tumoral cells containing low amounts of MG-IONP-DY647 nanoparticles internalized specifically through cell surface CCK2R causes apoptosis and cell death through a mechanism involving lysosome leaking and lysosomal cysteine proteases.

## DISCUSSION

In the context of increasing success of targeted therapy of cancers and accumulation of data showing overexpression of peptide receptors in several types of tumors as well as their contributing role in cancer development,<sup>33,34</sup> a synthetic analogue of gastrin was conjugated to iron oxide nanoparticles in order to produce a magnetic nanopatform for targeted therapy of tumors overexpressing CCK2R. The synthetic analogue of gastrin (MG) pharmacologically behaved similarly to CCK, the most efficient and potent natural agonist of CCK2R.<sup>35</sup>

We first showed that MG-IONP-DY647 nanoparticles, even at high concentrations, do not promote inflammation, as evidenced by the absence of IL-1 $\beta$  secretion by cultured macrophages. This result confirms the recognized good biocompatibility of iron oxide nanoparticles. Binding, uptake, and intracellular trafficking of MG-IONP-DY647 nanoparticles and the underlying cellular and molecular mechanisms were characterized on HEK293 cells, a reference cell model for characterization of membrane receptor internalization,

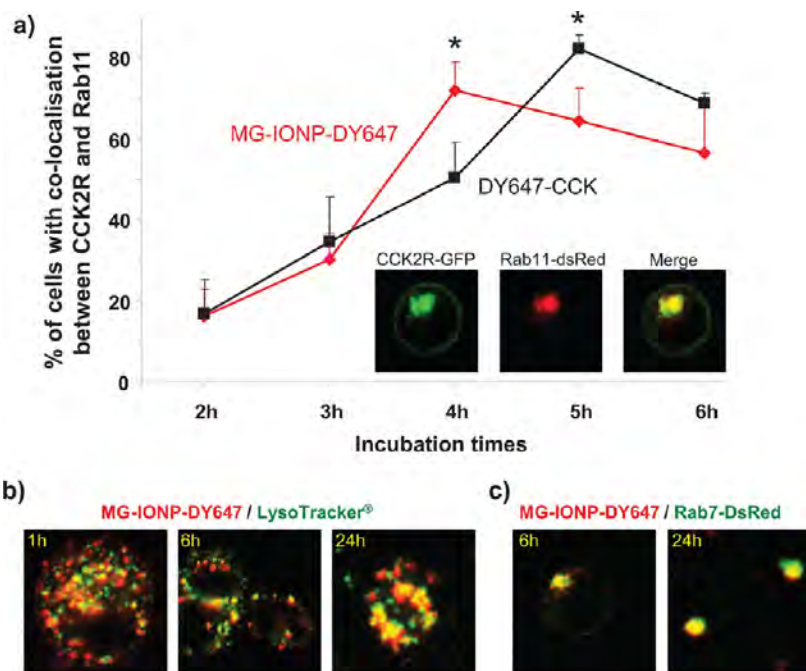


**Figure 7.** MG-IONP-DY647 accelerate slow recycling of internalized CCK2R and accumulate in lysosomes. (a) MG-IONP-DY647 modulate CCK2R recycling. HEK293 cells transiently coexpressing CCK2R-GFP and Rab11-dsRed were incubated with MG-IONP-DY647 nanoparticles ( $8 \mu\text{g Fe/mL}$ ) or CCK-DY647 ( $50 \text{ nM}$ ). Cells expressing both CCK2R-GFP and Rab11-dsRed were counted, and the percentage of cells presenting co-localization between the CCK2R-GFP and Rab11-dsRed was determined. Results are the mean  $\pm$  SEM of three distinct experiments with degree of confidence  $*0.01 < p < 0.05$ . In the inset, an example of confocal microscopy images of co-localization between CCK2R-GFP and Rab-11-DsRed is shown. (b, c) Internalized nanoconjugated MG-IONP-DY647 are directed to lysosomes. (b) Flp-In CCK2R-293 cells were preincubated with  $75 \mu\text{M}$  LysoTracker (green) for 30 min before incubation with MG-IONP-DY647. (c) Flp-In CCK2R-293 cells transiently expressing Rab7-DsRed (green) were incubated with MG-IONP-DY647.

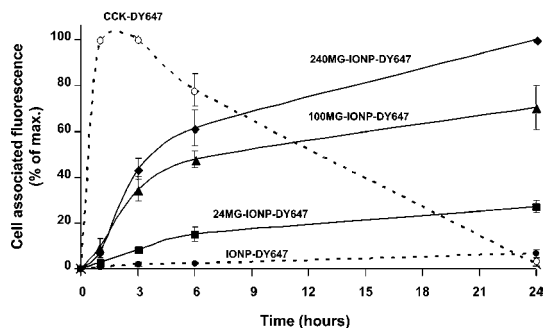


**Figure 8.** Time-course and specificity of uptake of MG-IONP-DY647 by tumoral endocrine cells InR1G9-CCK2R. InR1G9-CCK2R cells were incubated with MG-IONP-DY647 ( $16 \mu\text{g Fe/mL}$ ) or CCK-DY647 ( $0.1 \mu\text{M}$ ) for indicated times at  $37^\circ\text{C}$ . Kinetics are shown for nanoparticles without grafted MG (labeled as IONP-DY647) as well as for nanoparticles grafted with 24, 100, and 240 MG molecules per nanoparticle. Fluorescence was measured by flow cytometry, and results are expressed as % of maximum fluorescence associated with the cells and are the mean  $\pm$  SEM of three separate experiments.

as well as on tumoral cell lines (InR1G9) expressing or not CCK2R.<sup>32</sup> We found that MG-IONP-DY647 nanoparticles binding and internalization were entirely dependent on the presence of CCK2R at the cell surface. Nevertheless, kinetics of binding and internalization of MG-IONP-DY647 were much slower than that of fluorescent unconjugated CCK (CCK-DY647), although MG-IONP-DY647 nanoparticles internalized together

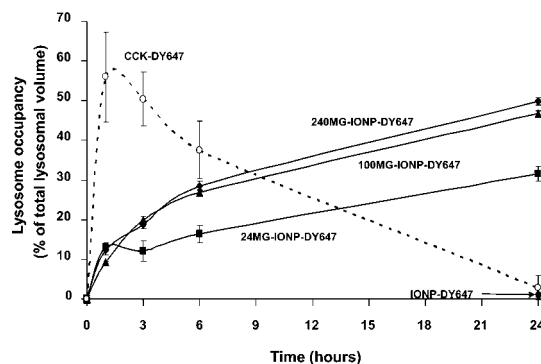


**Figure 9.** MG-IONP-DY647 trafficking to lysosomes of InR1G9 tumoral endocrine cells. InR1G9-CCK2R cells were incubated at  $37^\circ\text{C}$  with MG-IONP-DY647 ( $16 \mu\text{g Fe/mL}$ ), IONP-DY647 ( $16 \mu\text{g Fe/mL}$ ), or CCK-DY647 ( $0.1 \mu\text{M}$ ). LysoTracker ( $75 \text{ nM}$ ) was added 30 min before analysis on a confocal microscope. The presence of nanoparticles in lysosomes was quantified on the basis of co-localization between DY-647 and LysoTracker fluorescences using ImageJ software and Jacop Plugin. On average 2–3000 cells/experiment were analyzed. Results are the mean  $\pm$  SEM of three separate experiments.

with CCK2R through the initial molecular mechanism described for CCK- or gastrin-induced internalization of CCK2R.<sup>22</sup> Indeed, key steps in the internalization process such as  $\beta$ -arrestin2 recruitment and involvement of clathrin-coated pits and of dynamin were observed with both MG-IONP-DY647 (this study) and CCK-DY647.<sup>22</sup>

Analysis of CCK2R intracellular trafficking in HEK293 cells expressing either GFP-tagged CCK2R or DsRed-tagged

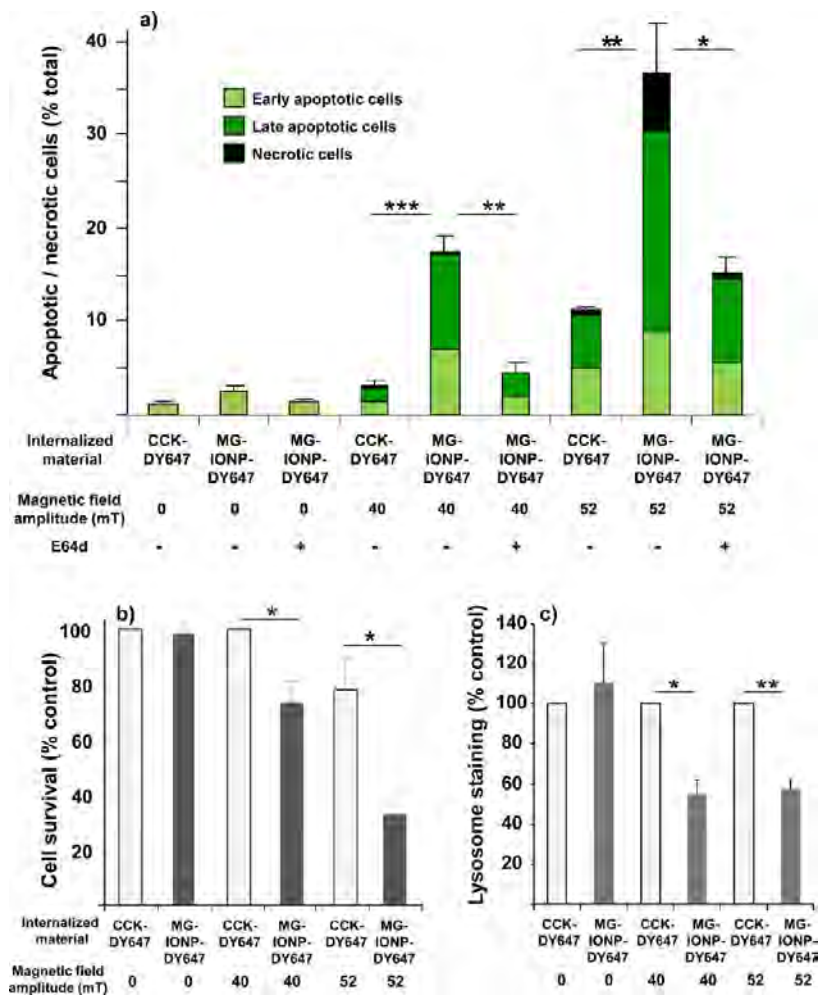


**Figure 10.** Internalized MG-IONP-DY647 by tumoral cells exposed to an alternating magnetic field induce apoptosis and cause cell death by affecting lysosome integrity. InR1G9-CCK2R cells were incubated with MG-IONP-DY647 (16  $\mu\text{g Fe/mL}$ ) or CCK-DY647 (0.1  $\mu\text{M}$ ) for 24 h at 37  $^{\circ}\text{C}$ . When indicated, E64d (10  $\mu\text{M}$ ) was added in the medium. Cells were then exposed for 2 h to an alternating magnetic field (275 kHz, 40 or 52 mT) at 37  $^{\circ}\text{C}$ . (a) Apoptotic and necrotic cells were counted 4 h after the end of magnetic field exposure by confocal microscopy analysis of cells labeled with FITC-annexin V and/or propidium iodide. Cells labeled only with FITC-annexin V were regarded as early apoptotic cells, those double-labeled with FITC-annexin/propidium iodide were regarded as late apoptotic cells, and those labeled only with propidium iodide were necrotic cells. (b) Cell survival was determined using MTT assay 24 h after the end of magnetic field exposure. (c) Lysosome staining with LysoTracker Red was determined 30 min after the end of magnetic field exposure. Results are the mean  $\pm$  SEM of three to five separate experiments. \*0.01 <  $p$  < 0.05; \*\*0.001 <  $p$  < 0.01; \*\*\* $p$  < 0.001.

Rab11, a small GTPase of slowly recycling vesicles, strongly supports that nanoconjugation of MG affected both the stability of the endocytotic complexes and CCK2R trafficking. Indeed, after stimulation with MG-IONP-DY647, CCK2R was found in vesicles distinct from that containing the nanoparticles and was targeted to recycling vesicles containing Rab11 earlier than CCK2R stimulated with unconjugated CCK or gastrin (Figures 6 and 7). These results are consistent with data showing that internalization and trafficking of a G-protein-coupled receptor are initially dictated by its ligand.<sup>36,37</sup>

Our data are in agreement with a report showing that nanoconjugation of an antibody directed against EGF receptor modulates antibody-induced internalization of this receptor.<sup>12</sup> Furthermore, it has been also shown that ligand dissociation from G-protein-coupled receptors (GPCRs) and subsequent degradation by

endosomal peptidases control trafficking and endosomal signaling of peptide receptors. For example, endothelin-converting enzyme 1 (ECE-1) rapidly degrades substance P, calcitonin gene-related peptide (CGRP), and somatostatin peptide in endosomes, disrupting the peptide-receptor- $\beta$ -arrestin complex and then allowing  $\beta$ -arrestins to return to the cytoplasm and receptors, to recycle.<sup>38–40</sup> For class B GPCRs such as CCK2R, dissociation from  $\beta$ -arrestin in endosomes is necessary for recycling and resensitization.<sup>37</sup> As an alternative hypothesis to explain the increased time-course of CCK2R localization in slowly recycling vesicles, CCK2R internalization as oligomers due to simultaneous binding of MG-IONP-DY647 to several receptor molecules at a time must be also considered. Such multiligand binding was described for neuropeptide Y1 receptor when targeted by neuropeptide Y-decorated quantum dots.<sup>11</sup>

---

Importantly, besides modifications of CCK2R trafficking, internalized MG-IONP-DY647 nanoparticles are directed to lysosomes, where they accumulate both in HEK293 and InR1G9 tumoral cells. Of interest, internalized MG-IONP-DY647 were much more stable in lysosomes than unconjugated fluorescent CCK, which became almost nondetectable after 24 h of contact with the cells.

Last, we started to explore the opportunity offered by magnetic nanoparticles accumulated into lysosomes of tumoral cells to act as a therapeutic agent inducing cell death upon exposure to an alternating magnetic field. The results that were obtained clearly demonstrate that exposure of tumoral cells containing actively internalized MG-IONP-DY647 to an alternating magnetic field of moderate strength causes apoptosis followed by cell death. Moreover, first data on the mechanisms at the origin of cell death support the involvement of lysosomes and cysteine proteases, since staining of lysosomes with pH-independent LysoTracker Red was diminished by exposure of cells containing targeted nanoparticles to a magnetic field. Moreover, E64d inhibitor was able to reverse the effect of the magnetic field on apoptosis. On this basis, and according to our current knowledge, lysosome membrane permeabilization followed by leaking of cathepsin B is likely at the origin of tumoral cell death. Thus, MG-IONP-DY647 exposed to an alternating magnetic field behaved as a lysosomotropic agent in tumoral endocrine cells. Several other agents have been shown to induce lysosome membrane permeabilization and subsequent activation of lysosomal death pathways.<sup>24</sup> EGF-grafted iron nanoparticles internalized by tumoral cells and exposed to an alternating magnetic field were previously reported to cause lysosomal membrane permeabilization, together with production of reactive oxygen species (ROS) and subsequent cell death.<sup>13</sup> It is worthy to note that ROS formation, lysosomal membrane permeabilization, and cell death occurred in the absence of any perceptible temperature rise in the incubation medium of the cells (refs 13, 14, and 18 and this study). These experimental data, as well as basic calculations,<sup>41,42</sup> support the view that minute amounts of nanoparticles located in lysosomes are unable to elicit temperature rise, including inside the cells. Alternatively, local temperature increase,<sup>15,43</sup> nanoparticle rotation,<sup>13</sup> or nanoparticle high-frequency motion<sup>44</sup> has been proposed.

Whatever the initial mechanism at the origin of lysosomal membrane permeabilization, data from the

current study highlight the feasibility of cell death induction with very small quantities of actively and specifically internalized nanoparticles. Basic calculation using the model presented in ref 45 indicates that inducing a temperature increase of 5 °C in a 3 mm size tumor with MG-IONP-DY647 would require approximately 165 pg Fe/cell, which is a completely unrealistic objective using targeted nanoparticles which are internalized only *via* cell surface receptors. Here, a maximum of 2.2 pg Fe/cell could be specifically internalized *via* cell surface CCK2R receptors. Although this low amount of nanoparticles was sufficient to induce cell death, it likely explains, together with the low heating power of the iron oxide nanoparticles, the relatively modest level of cell death achieved in this study using a magnetic field of 40 mT. Our results show that increasing the amplitude of the magnetic field from 40 mT to 52 mT augmented the death rate of cells containing nanoparticles. However, such a treatment also caused damage to cells that had not accumulated nanoparticles. Therefore, optimization of the nanoparticles will be required in order to enhance their killing efficiency. Their size and composition could be changed to increase their heating power.

## CONCLUSIONS

Grafting of gastrin to iron oxide nanoparticles enabled highly specific targeting of HEK293 and tumoral endocrine cells INR1G9 expressing CCK2R, a G-protein-coupled receptor overexpressed in endocrine tumors. Subsequently, nanoparticles undergo internalization with CCK2R through a mechanism involving  $\beta$ -arrestins, clathrin-coated pits, and dynamin composing the endocytotic machinery of CCK2R. Internalized nanoparticles are then directed to lysosomes, where they accumulate in minute amount (2.2 pg Fe/cell). Application of an alternating magnetic field to cells containing MG-IONP-DY647 induced apoptosis and cell death through a lysosomal death pathway, demonstrating that cell death is triggered even though nanoparticles of low thermal power are internalized in minute amounts by the cells. These data are very promising in light of the recent concept that lysosomal membrane permeabilization could be an effective way to kill apoptosis-resistant cancer cells.<sup>24</sup> Together with previous pioneer findings,<sup>13,14</sup> they represent a solid basis for future studies aimed at establishing the proof-of-concept of nanotherapy of cancers using ligand-grafted magnetic nanoparticles specifically internalized *via* their cell surface receptors.

---

## MATERIALS AND METHODS

**Chemical and Biological Materials.** Iron oxide nanoparticles were purchased from Genovis (Lund, Sweden). The characteristics of these IONP provided by the manufacturer are given in Supporting Information Table 1. A stable replicate of CCK, sulfated [Thr28,Nle31]-CCK 25-33, was kindly given by Prof. L. Moroder<sup>46</sup>

and is referred to as CCK. <sup>125</sup>I-Sodium (2000 Ci/mmol) and [myo-3H]inositol (5  $\mu$ Ci/mL) were from Perkin-Elmer Life Sciences. CCK was conjugated with Bolton-Hunter reagent, purified, and radioiodinated as described previously<sup>47</sup> and is referred to as <sup>125</sup>I-CCK. Gastrin replicate termed MG (Figure 1) was synthesized by Covalab (Villeurbanne, France). DY647-tagged CCK and MG were obtained according to the procedure described for



glucose insulinotropic polypeptide by coupling the peptides to NHS-DY647-PEG1 (Dyomics GmbH, Jena, Germany)<sup>48</sup> and are referred to as CCK-DY647 and MG-DY647, respectively. The following products were supplied as follows: 3-maleimidopropionic acid *N*-hydroxysuccinimide ester (Thermo Scientific), magnetic columns (Miltenyi, Berisch, Gladback, Germany), specific inhibitor of dynamin, dynasore (Calbiochem), an inhibitor of clathrin-dependent uptake, chlorpromazine (Sigma-Aldrich), an inhibitor of caveoles, filipin (Sigma), and LysoTracker (Invitrogen).

The cDNA encoding CCK2R was subcloned in pcDNA3 vector, and green fluorescent protein (GFP)-tagged CCK2R was generated by subcloning the CCK2R cDNA in pEGFP-N1 (BD Biosciences Clontech). DsRed-tagged Rab11, DsRed-tagged Rab7, and clathrin-LCa-eYFP were obtained from Addgene (www.addgene.org). GFP-tagged  $\beta$ -arrestin2 was kindly supplied by Robert Lefkowitz (Duke University Medical Center, Durham, NC, USA). The annexin V binding apoptosis assay kit was from AAT Bioquest, Inc. (Sunnyvale, CA, USA). Cell lines were HEK 293 cells stably expressing CCK2R (Flp-In CCK2R-293) obtained using the Flp-In system (HEK293) (Invitrogen) as previously described;<sup>22</sup> the glucagon-producing hamster tumoral cell line InR1G9 stably expressing CCK2R obtained as previously described (InR1G9-CCK2R),<sup>32</sup> and the Raw 264.7 mouse leukemic monocyte macrophage cell line. Lab-Tek II chambers were from Thermo Fisher (Rochester, NY, USA), and glass-bottom Cellview dishes were from Greiner Bio-one, Courtaboeuf, France.

**Preparation of Gastrin-Decorated Magnetic Nanoparticles (MG-IONP-DY647).** The protocol used for grafting 100 molecules of MG per IONP was as follows: an aliquot of IONP (80  $\mu$ L of IONP at a concentration of 12 mg Fe<sub>3</sub>O<sub>4</sub>/mL) was added to 120  $\mu$ L of sodium phosphate buffer (0.2 M Na<sub>2</sub>HPO<sub>4</sub> pH 7.3, 150 mM NaCl) and sonicated for 10 min on melting ice (Bioblock Scientific 88154). NHS-DY647-PEG1 (12  $\mu$ g) in solution in dimethyl formamide (24  $\mu$ L) was added and allowed to react for 2 h at room temperature. Then, 53  $\mu$ g of 3-maleimidopropionic acid *N*-hydroxysuccinimide ester in solution in 10  $\mu$ L of DMF was added and incubated at room temperature for 1 h. MG (100  $\mu$ L of a solution of 30% DMF, 70% H<sub>2</sub>O containing 20  $\mu$ g of peptide) was added to IONP and allowed to react for 2 h. Finally, free maleimide functions were saturated by addition of an excess of cystein (62  $\mu$ g in 50  $\mu$ L of reaction buffer). Grafted nanoparticles were recovered through a magnet column in H<sub>2</sub>O. MG-IONP-DY647 were stored at 4 °C. Before use, MG-IONP-DY647 were always sonicated on ice for 10 min. The amount of recovered nanoparticles was determined by magnetic measurement (see below), and the density of grafted MG at the nanoparticle surface was assessed by measuring the ability of different dilutions of MG-IONP-DY647 to stimulate production of inositol phosphates in Flp-In CCK2R-293 cells. The density of MG was calculated from a dose–response curve with free MG (Supplementary Figure 1b).

**Dynamic Light Scattering Measurements of Hydrodynamic Diameter.** A suspension of iron nanoparticles at 0.1 mg/mL was prepared in RPMI 1640 medium containing 0.5% FBS. The iron nanoparticle suspension was sonicated for 10 min on ice. After temperature equilibrium to 20 °C, the particle size was measured by dynamic light scattering using Nanotracs 250 (Microtrac, York, PA, USA).

**Specific Absorption Rate Measurements.** A 300  $\mu$ L solution of IONPs at 5.9 mg Fe/mL was used for specific absorption rate measurements. The temperature increase of the sample placed in a 275 kHz alternating magnetic field delivered by a commercial magnetic inductor (Fives Celes, Lautenback, France) during 100 s was measured. A blank sample containing water was used in parallel in order to remove the contribution of eddy current to the temperature increase. Temperature measurements were performed using a thermal probe (Reflex, Neoptix, Canada). The specific absorption rate was calculated using standard formula and taking into account the specific heat of water.

**Determination of Iron Concentrations and Amounts.** Amounts of iron were determined by magnetic measurements using a vibrating sample magnetometer (PPMS, Quantum Design, USA). First, we checked the value of concentration and saturation

magnetization provided by the manufacturer by performing magnetic measurements on a dried powder of MG-IONP-DY647. Hysteresis cycles at 270 K were measured, and the linear slope corresponding to the diamagnetic signal was removed from the raw measurement. The remaining signal was fitted with a distribution of Langevin functions in parallel with a fit of the NP size distribution obtained by TEM. The magnetization and concentration values determined from this fit are  $73 \pm 10$  Am<sup>2</sup>/kg Fe<sub>3</sub>O<sub>4</sub> and  $2.1 \pm 0.2$  mg/mL, respectively, when  $80$  Am<sup>2</sup>/kg Fe<sub>3</sub>O<sub>4</sub> and 2 mg/mL were expected from manufacturer data. We thus considered manufacturer data as reliable and used them in the following. To determine iron content in cells, a suspension containing a known number of dried cells ( $2.5 \pm 0.2 \times 10^6$ ) was put into a magnetic measurement capsule, the excess of liquid removed, and the remaining liquid allowed to evaporate. Hysteresis loops were measured at 300 K at a magnetic field of 5 T. The obtained magnetization was divided by the saturation magnetization of the nanoparticles provided by the nanoparticle supplier (107 Am<sup>2</sup>/kg Fe) and the number of cells to obtain the iron content per cell.

**Transmission Electron Microscopy.** Flp-In CCK2R-293 or HEK293 cells were grown in poly-L-lysine-coated wells and incubated with MG-IONP-DY647 (8  $\mu$ g Fe/mL) for indicated times in phosphate-buffered saline (PBS) 0.2% BSA. After two washes, cells were fixed with 4% glutaraldehyde in Sorensen buffer for 4 h at 4 °C. After washes, cells were postfixed in 1% osmium tetroxide (osmium 2%, saccharose 0.25 M, Sorensen 0.05 M) for 1 h at 20 °C, followed by washings with distilled water and uranyl acetate 2% for 12 h at 4 °C. After dehydration, 70 nm sections of cells embedded in EMBED 812 resin were stained with uranyl acetate and lead citrate and examined with a TEM (Hitachi HU12A, Japan) operating at 75 kV.

**Cell Culture and Transfections.** Flp-In CCK2R-293 and HEK293 cells were cultured in Dulbecco's modified Eagle's medium (DMEM) containing 10% FBS and 1% penicillin–streptomycin (Invitrogen). InR1G9 and Raw cells were cultured in RPMI 1640 medium containing 10% fetal bovine serum (FBS) and 1% penicillin–streptomycin (Invitrogen). Cells were grown in a humidified atmosphere at 95% air and 5% CO<sub>2</sub>. Transfections of HEK293 cells were carried out using polyethyleneimine (Polyscience) on 10 cm dishes containing  $2.0 \times 10^6$  cells, which were seeded 24 h before transfection. Plasmids containing cDNA encoding GFP-tagged CCK2R,  $\beta$ -arrestin2-GFP, Rab7-DsRed, Rab11-DsRed, or clathrin-LCa-eYFP were transfected.

**Analysis of Macrophage Inflammation Activation.** To evaluate IL-1 $\beta$  secretion, Raw 264.7 macrophages were primed with ultrapure lipopolysaccharide (LPS, 500 ng/mL) (Invivogen, Toulouse, France), for 4 h. This step of LPS stimulation triggers synthesis and intracellular accumulation of pro-IL-1 $\beta$ .<sup>49</sup> Medium was removed and cells were washed twice with PBS. Then, Raw 264.7 cells were stimulated with IONP-MG-DY647 or silica nanoparticles for 6 h at 37 °C. This second step of stimulation is expected to assemble a multiprotein complex termed an inflammasome, leading to enzymatic cleavage of pro-IL1 $\beta$  by caspase-1 and release of its active form, IL1 $\beta$ .<sup>49</sup> Supernatants were recovered and assayed for IL-1 $\beta$  secretion with an ELISA kit according to the manufacturer's instructions.

**Receptor Binding and Inositol Phosphate Assays.** Cells were plated onto 24-well plates and grown for 24 h. Binding assays were performed on attached cells using <sup>125</sup>I-CCK according to the protocol previously described in detail.<sup>50</sup> IC<sub>50</sub> values were calculated from homologous <sup>125</sup>I-CCK competition binding experiments using the nonlinear curve-fitting software GraphPad Prism (San Diego, CA, USA). Inositol phosphate production was determined as previously described after 24 h of incubation in DMEM containing 2  $\mu$ Ci/mL of myo-[2-<sup>3</sup>H]inositol (specific activity: 10–25 Ci/mmol).<sup>50</sup>

**Quantification of MG-IONP-DY647 Binding and Uptake by Flow Cytometry.** Cells were seeded onto poly-L-lysine-coated 12-well plates at a density of  $150 \times 10^3$  cells/well and grown for 24 h on RPMI 1640 medium containing 2% FBS. MG-IONP-DY647 (4 to 8  $\mu$ g of Fe) or CCK-DY647 (0.1  $\mu$ M) in 250  $\mu$ L of medium were added and incubated at 37 °C in a 5% CO<sub>2</sub> atmosphere for the desired times. Then, cells were rinsed twice with ice-cold PBS containing 0.5% BSA and once with PBS alone. Cells were recovered and

transferred to FACS tubes. Cell-associated fluorescence was determined using a BD FACSCalibur flow cytometer. In parallel, samples of cells were collected for magnetic determination of iron.

**Internalization and Trafficking Studies.** Internalization and trafficking of nanoparticles were characterized using a Zeiss laser scanning microscope (LSM-510). Routinely, cells that had been eventually transfected 24 h earlier were plated ( $\sim 80\text{--}100 \times 10^3$  cells/compartiment) onto poly-L-lysine-coated four-compartment Cellview or Lab-Tek chambered coverglass. After overnight growth, cells were rinsed with PBS and incubated with MG-IONP-DY647 (4 to 16  $\mu\text{g Fe/mL}$ ) or CCK-DY647 (0.1 or 0.01  $\mu\text{M}$ ) in 250  $\mu\text{L}$  of PBS containing 0.5% BSA (for HEK cells) or RPMI 1640 medium containing 10% FBS and 1% penicillin–streptomycin (for INR1G9 cells) completed or not with inhibitors. For lysosome staining, cells were incubated for 30 min in the presence of 75 nM LysoTracker Red DND-99 prior to stimulation with nanoparticles or CCK-DY647. Collected images were analyzed using ImageJ software and the Jacop plugin, which provided cytofluorograms and Pearson's and overlap coefficients that account for co-localization.

**Cell Treatment by an Alternating Magnetic Field.** Cells were seeded 24 h before the experiments onto four-compartment Cellview dishes at a density of  $\sim 80 \times 10^3$  cells/compartiment in RPMI 1640 medium containing 10% FBS and 1% penicillin–streptomycin. Cells were rinsed with PBS and incubated with MG-IONP-DY647 (16  $\mu\text{g Fe/mL}$ ) or DY647 (0.1  $\mu\text{M}$ ) for 24 h at 37 °C in RPMI 1640 buffered with 10 mM Hepes buffer pH 7.4 and containing 0.5% FBS and 1% penicillin–streptomycin with or without protease inhibitors E64d (10  $\mu\text{M}$ ), pepstatin A (100  $\mu\text{M}$ ), or chloroquine (25  $\mu\text{M}$ ). Incubation medium was withdrawn, and cells were rinsed twice with incubation medium. Attached cells were exposed to an alternating magnetic field (275 kHz, 40 or 52 mT) delivered by a commercial magnetic inductor (Fives Celes, Lautenback, France) for 2 h. The magnetic field amplitude was measured by a homemade pick-up coil. The latter was calibrated by measuring the high-frequency magnetic field on an electromagnet in which the current/magnetic field relationship was calibrated in dc and the ac current could be accurately measured using a noncontact ac current probe (Tektronix, P6021).<sup>51</sup> The inner diameter of the coil was 3.5 cm so that the Cellview dish fit in its middle. The magnetic field was applied in the plane of the Cellview dish. The temperature of the Cellview dish was controlled using a thermal probe (Reflex, Neoptix, Canada) placed in the incubation medium of the cells. The temperature of the Cellview dish was maintained at  $37.0 \pm 0.4$  °C thanks to an air gun placed below it. Control samples were also maintained out of the cell incubator during hyperthermia experiments, and their temperature was regulated similarly to the assay samples. At the end of the experiments, cells were placed in a humidified atmosphere at 5% CO<sub>2</sub> at 37 °C for 4 h.

**Determination of Apoptosis and Cell Death.** The effects of magnetic field treatment were investigated as follows: first, apoptotic and necrotic cells labeled with FITC-annexinV and/or propidium iododure (Cell Meter Annexin V apoptosis 832 assay kit, AAT Bioquest) were counted 4 h after the end of magnetic field exposure. Counting of labeled cells was carried out by analyzing confocal microscopy images representing populations of 2–3000 cells/experiment using ImageJ software. Lysosome integrity was determined using LysoTracker Red staining reagent, which was added (at 75 nM) to cells at the beginning of the magnetic field runs. Quantification of staining was performed 30 min later by analyzing 2–3000 cells/experiment using Morpho Expert software (Explora Nova, La Rochelle, France). Cell death was determined 24 h post-magnetic field treatment using a MTT viability assay (MTT: [(3-(4,5-dimethylthiazol-2-yl)-2,5-diphenyltetrazolium bromide), Sigma-Aldrich].

**Conflict of Interest:** The authors declare no competing financial interest.

**Acknowledgment.** We thank Cellular Imaging Facility Ranguel and Flow Cytometry platform of I2MC/INSERM for the excellent technical support. This research was partly funded

by Ligue Nationale Contre le Cancer, the European Community's Seventh Framework Programm under grant agreement no. 262943 "MULTIFUN" and INSERM grant no. PC201310.

**Supporting Information Available:** Supporting Information including supplementary figures and legends to these figures is available free of charge via the Internet at <http://pubs.acs.org>.

## REFERENCES AND NOTES

- Peer, D.; Karp, J. M.; Hong, S.; Farokhzad, O. C.; Margalit, R.; Langer, R. Nanocarriers as an Emerging Platform for Cancer Therapy. *Nat. Nanotechnol.* **2007**, *2*, 751–760.
- Yoo, D.; Lee, J. H.; Shin, T. H.; Cheon, J. Theranostic Magnetic Nanoparticles. *Acc. Chem. Res.* **2011**, *44*, 863–874.
- Schutz, C. A.; Juillerat-Jeanneret, L.; Mueller, H.; Lynch, I.; Riediker, M. Therapeutic Nanoparticles in Clinics and under Clinical Evaluation. *Nanomedicine (London, U.K.)* **2013**, *8*, 449–467.
- Corot, C.; Robert, P.; Idee, J. M.; Port, M. Recent Advances in Iron Oxide Nanocrystal Technology for Medical Imaging. *Adv. Drug Delivery Rev.* **2006**, *58*, 1471–1504.
- Ferrari, M. Cancer Nanotechnology: Opportunities and Challenges. *Nat. Rev. Cancer* **2005**, *5*, 161–171.
- Murthy, S. K. Nanoparticles in Modern Medicine: State of the Art and Future Challenges. *Int. J. Nanomed.* **2007**, *2*, 129–141.
- Figuerola, A.; Di Corato, R.; Manna, L.; Pellegrino, T. From Iron Oxide Nanoparticles towards Advanced Iron-Based Inorganic Materials Designed for Biomedical Applications. *Pharmacol. Res.* **2010**, *62*, 126–143.
- Hilger, I.; Kaiser, W. A. Iron Oxide-Based Nanostructures for MRI and Magnetic Hyperthermia. *Nanomedicine (London, U.K.)* **2012**, *7*, 1443–1459.
- Mahon, E.; Salvati, A.; Baldelli Bombelli, F.; Lynch, I.; Dawson, K. A. Designing the Nanoparticle-Biomolecule Interface for "Targeting and Therapeutic Delivery". *J. Controlled Release* **2012**, *161*, 164–174.
- Almeida, J. P.; Chen, A. L.; Foster, A.; Drezek, R. *In Vivo* Biodistribution of Nanoparticles. *Nanomedicine (London, U.K.)* **2011**, *6*, 815–835.
- Hild, W.; Pollinger, K.; Caporale, A.; Cabrele, C.; Keller, M.; Pluym, N.; Buschauer, A.; Rachel, R.; Tessmar, J.; Breunig, M.; *et al.* G Protein-Coupled Receptors Function as Logic Gates for Nanoparticle Binding and Cell Uptake. *Proc. Natl. Acad. Sci. U.S.A.* **2010**, *107*, 10667–10672.
- Bhattacharyya, S.; Bhattacharya, R.; Curley, S.; McNiven, M. A.; Mukherjee, P. Nanoconjugation Modulates the Trafficking and Mechanism of Antibody Induced Receptor Endocytosis. *Proc. Natl. Acad. Sci. U.S.A.* *107*, 14541–14546.
- Domenech, M.; Marrero-Berrios, I.; Torres-Lugo, M.; Rinaldi, C. Lysosomal Membrane Permeabilization by Targeted Magnetic Nanoparticles in Alternating Magnetic Fields. *ACS Nano* **2013**, *7*, 5091–5101.
- Creixell, M.; Bohorquez, A. C.; Torres-Lugo, M.; Rinaldi, C. EGFR-Targeted Magnetic Nanoparticle Heaters Kill Cancer Cells without a Perceptible Temperature Rise. *ACS Nano* **2011**, *5*, 7124–7129.
- Riedinger, A.; Guardia, P.; Curcio, A.; Garcia, M. A.; Cingolani, R.; Manna, L.; Pellegrino, T. Subnanometer Local Temperature Probing and Remotely Controlled Drug Release Based on Azo-Functionalized Iron Oxide Nanoparticles. *Nano Lett.* **2013**, *13*, 2399–2406.
- Johannsen, M.; Thiesen, B.; Wust, P.; Jordan, A. Magnetic Nanoparticle Hyperthermia for Prostate Cancer. *Int. J. Hyperthermia* **2010**, *26*, 790–795.
- Silva, A. C.; Oliveira, T. R.; Mamani, J. B.; Malheiros, S. M.; Malavolta, L.; Pavon, L. F.; Sibov, T. T.; Amaro, E., Jr.; Tannus, A.; Vidoto, E. L.; *et al.* Application of Hyperthermia Induced by Superparamagnetic Iron Oxide Nanoparticles in Glioma Treatment. *Int. J. Nanomed.* **2011**, *6*, 591–603.
- Villanueva, A.; de la Presa, P.; Alonso, J. M.; Rueda, T.; Martinez, A.; Crespo, P.; Morales, M. P.; Gonzalez-Fernandez, M. A.; Valdes, J.; Rivero, G. Hyperthermia HeLa

- Cell Treatment with Silica-Coated Manganese Oxide Nanoparticles. *J. Phys. Chem. C* **2010**, *114*, 1976–1981.
19. Reubi, J. C. Targeting CCK Receptors in Human Cancers. *Curr. Top. Med. Chem.* **2007**, *7*, 1239–1242.
  20. Reubi, J. C.; Maecke, H. R. Peptide-Based Probes for Cancer Imaging. *J. Nucl. Med.* **2008**, *49*, 1735–1738.
  21. Reubi, J. C.; Waser, B. Unexpected High Incidence of Cholecystokinin-B/Gastrin Receptors in Human Medullary Thyroid Carcinomas. *Int. J. Cancer* **1996**, *67*, 644–647.
  22. Magnan, R.; Masri, B.; Escrieut, C.; Foucaud, M.; Cordelier, P.; Fourmy, D. Regulation of Membrane Cholecystokinin-2 Receptor by Agonists Enables Classification of Partial Agonists as Biased Agonists. *J. Biol. Chem.* **2011**, *286*, 6707–6719.
  23. Magnan, R.; Escrieut, C.; Gigoux, V.; De, K.; Clerc, P.; Niu, F.; Azema, J.; Masri, B.; Cordomi, A.; Baltas, M.; et al. Distinct CCK-2 Receptor Conformations Associated with beta-Arrestin-2 Recruitment or Phospholipase-C Activation Revealed by a Biased Antagonist. *J. Am. Chem. Soc.* **2013**, *135*, 2560–2573.
  24. Groth-Pedersen, L.; Jaattela, M. Combating Apoptosis and Multidrug Resistant Cancers by Targeting Lysosomes. *Cancer Lett.* **2010**, *332*, 265–274.
  25. Behe, M.; Kluge, G.; Becker, W.; Gotthardt, M.; Behr, T. M. Use of Polyglutamic Acids to Reduce Uptake of Radiometal-Labeled Minigastrin in the Kidneys. *J. Nucl. Med.* **2005**, *46*, 1012–1015.
  26. Laverman, P.; Joosten, L.; Eek, A.; Roosenburg, S.; Peitl, P. K.; Maina, T.; Macke, H.; Aloj, L.; von Guggenberg, E.; Sosabowski, J. K.; et al. Comparative Biodistribution of 12 (1)(1)In-Labelled Gastrin/CCK2 Receptor-Targeting Peptides. *Eur. J. Nucl. Med. Mol. Imaging* **2011**, *38*, 1410–1416.
  27. Daldrup-Link, H. E.; Golovko, D.; Ruffell, B.; Denardo, D. G.; Castaneda, R.; Ansari, C.; Rao, J.; Tikhomirov, G. A.; Wendland, M. F.; Corot, C.; et al. MRI of Tumor-Associated Macrophages with Clinically Applicable Iron Oxide Nanoparticles. *Clin. Cancer Res.* **17**, 5695–5704.
  28. Levy, M.; Luciani, N.; Alloyeau, D.; Elgrabli, D.; Deveaux, V.; Pechoux, C.; Chat, S.; Wang, G.; Vats, N.; Gendron, F.; et al. Long Term *In Vivo* Biotransformation of Iron Oxide Nanoparticles. *Biomaterials* **32**, 3988–3999.
  29. Yazdi, A. S.; Guarda, G.; Riteau, N.; Drexler, S. K.; Tardivel, A.; Couillin, I.; Tschopp, J. Nanoparticles Activate the NLR Pyrin Domain Containing 3 (Nlrp3) Inflammasome and Cause Pulmonary Inflammation through Release of IL-1Alpha and IL-1Beta. *Proc. Natl. Acad. Sci. U.S.A.* **107**, 19449–19454.
  30. Stenmark, H. Rab GTPases as Coordinators of Vesicle Traffic. *Nat. Rev. Mol. Cell Biol.* **2009**, *10*, 513–525.
  31. Kallunki, T.; Olsen, O. D.; Jaattela, M. Cancer-Associated Lysosomal Changes: Friends or Foes? *Oncogene* **2013**, *32*, 1995–2004.
  32. Leung-Theung-Long, S.; Roulet, E.; Clerc, P.; Escrieut, C.; Marchal-Victorion, S.; Ritz-Laser, B.; Philippe, J.; Pradayrol, L.; Seva, C.; Fourmy, D.; et al. Essential Interaction of Egr-1 at an Islet-Specific Response Element for Basal and Gastrin-Dependent Glucagon Gene Transactivation in Pancreatic Alpha-Cells. *J. Biol. Chem.* **2005**, *280*, 7976–7984.
  33. Reubi, J. C. Peptide Receptors as Molecular Targets for Cancer Diagnosis and Therapy. *Endocr. Rev.* **2003**, *24*, 389–427.
  34. Dorsam, R. T.; Gutkind, J. S. G-Protein-Coupled Receptors and Cancer. *Nat. Rev. Cancer* **2007**, *7*, 79–94.
  35. Dufresne, M.; Seva, C.; Fourmy, D. Cholecystokinin and Gastrin Receptors. *Physiol. Rev.* **2006**, *86*, 805–847.
  36. Violin, J. D.; Lefkowitz, R. J. Beta-Arrestin-Biased Ligands at Seven-Transmembrane Receptors. *Trends Pharmacol. Sci.* **2007**, *28*, 416–422.
  37. Murphy, J. E.; Padilla, B. E.; Hasdemir, B.; Cottrell, G. S.; Bunnett, N. W. Endosomes: A Legitimate Platform for the Signaling Train. *Proc. Natl. Acad. Sci. U.S.A.* **2009**, *106*, 17615–17622.
  38. Padilla, B. E.; Cottrell, G. S.; Roosterman, D.; Pikiros, S.; Muller, L.; Steinhoff, M.; Bunnett, N. W. Endothelin-Converting Enzyme-1 Regulates Endosomal Sorting of Calcitonin Receptor-Like Receptor and Beta-Arrestins. *J. Cell Biol.* **2007**, *179*, 981–997.
  39. Roosterman, D.; Cottrell, G. S.; Padilla, B. E.; Muller, L.; Eckman, C. B.; Bunnett, N. W.; Steinhoff, M. Endothelin-Converting Enzyme 1 Degrades Neuropeptides in Endosomes to Control Receptor Recycling. *Proc. Natl. Acad. Sci. U.S.A.* **2007**, *104*, 11838–11843.
  40. Roosterman, D.; Kempkes, C.; Cottrell, G. S.; Padilla, B. E.; Bunnett, N. W.; Turk, C. W.; Steinhoff, M. Endothelin-Converting Enzyme-1 Degrades Internalized Somatostatin-14. *Endocrinology* **2008**, *149*, 2200–2207.
  41. Carrey, J.; Mehdaoui, B.; Respaud, M. Simple Models for Dynamic Hysteresis Loop Calculations of Magnetic Single-Domain Nanoparticles: Application to Magnetic Hyperthermia Optimization. *J. Appl. Phys.* **2011**, *110*, 039902–039902-1.
  42. Mehdaoui, B.; Meffre, A.; Carrey, J.; Lachaize, S.; Lacroix, L. M.; Gougeon, M.; Chaudret, B.; Respaud, M. Optimal Size of Nanoparticles for Magnetic Hyperthermia: A Combined Theoretical and Experimental Study. *Adv. Funct. Mater.* **2011**, *21*, 4573–4581.
  43. Huang, H.; Delikanli, S.; Zeng, H.; Ferkey, D. M.; Pralle, A. Remote Control of Ion Channels and Neurons through Magnetic-Field Heating of Nanoparticles. *Nat. Nanotechnol.* **2010**, *5*, 602–606.
  44. Carrey, J.; Connord, V.; Respaud, M. Ultrasound Generation and High-Frequency Motion of Magnetic Nanoparticles in an Alternating Magnetic Field: Toward Intracellular Ultrasound Therapy? *Appl. Phys. Lett.* **2013**, *102*, 232404–1–232404-5.
  45. Hergt, R.; Dutz, S. Magnetic Particle Hyperthermia-Biophysical Limitations of a Visionary Tumour Therapy. *J. Magn. Magn. Mater.* **2007**, *311*, 187–192.
  46. Moroder, L.; Wilschowitz, L.; Gemeiner, M.; Gohring, W.; Knof, S.; Scharf, R.; Thamm, P.; Gardner, J. D.; Solomon, T. E.; Wunsch, E. [Cholecystokinin-Pancreozymin Synthesis. Synthesis of [28-Threonine,31-Norleucine]- and [28-Threonine,31-Leucine]Cholecystokinin-Pancreozymin-(25–33)-Nonapeptide]. *Hoppe Seylers Z. Physiol. Chem.* **1981**, *362*, 929–942.
  47. Fourmy, D.; Lopez, P.; Poirot, S.; Jimenez, J.; Dufresne, M.; Moroder, L.; Powers, S. P.; Vaysse, N. A New Probe for Affinity Labelling Pancreatic Cholecystokinin Receptor with Minor Modification of its Structure. *Eur. J. Biochem.* **1989**, *185*, 397–403.
  48. Yaqub, T.; Tikhonova, I. G.; Lattig, J.; Magnan, R.; Laval, M.; Escrieut, C.; Boulegue, C.; Hewage, C.; Fourmy, D. Identification of Determinants of Glucose-Dependent Insulinotropic Polypeptide Receptor that Interact with N-Terminal Biologically Active Region of the Natural Ligand. *Mol. Pharmacol.* **2010**, *77*, 547–58.
  49. Martinon, F.; Mayor, A.; Tschopp, J. The Inflammasomes: Guardians of the Body. *Annu. Rev. Immunol.* **2009**, *27*, 229–265.
  50. Foucaud, M.; Marco, E.; Escrieut, C.; Low, C.; Kalindjian, B.; Fourmy, D. Linking Non-Peptide Ligand Binding Mode to Activity at the Human Cholecystokinin-2 Receptor. *J. Biol. Chem.* **2008**, *283*, 35860–35868.
  51. Lacroix, L. M.; Carrey, J.; Respaud, M. A Frequency-Adjustable Electromagnet for Hyperthermia Measurements on Magnetic Nanoparticles. *Rev. Sci. Instrum.* **2008**, *79*, 093909-1–5.